Understanding artificial optical magnetism of periodic metal-dielectric-metal layered structures

C. Tserkezis,[1] N. Papanikolaou,[2] G. Gantzounis,[1] and N. Stefanou[1]
[1]*Section of Solid State Physics, University of Athens, Panepistimioupolis, GR-157 84 Athens, Greece*
[2]*Institute of Microelectronics, NCSR "Demokritos," GR-153 10 Athens, Greece*
(Received 11 June 2008; revised manuscript received 19 September 2008; published 14 October 2008)

Plasmonic excitations in two- and three-dimensional ordered assemblies of metal-dielectric-metal nanosandwiches are studied by means of full-electrodynamic calculations using the layer-multiple-scattering method. Plasmon hybridization results in collective electric-dipole-like and magnetic-dipole-like resonant modes, which are directly controlled by the lattice constant and the geometrical characteristics of the building units. It is shown that, in planar arrays of such composite nanoparticles on a dielectric substrate, the magnetic resonance induces a negative effective permeability, as large as −2, which can be tuned within the range of near-infrared and visible frequencies. However, as successive layers are stacked together to build a three-dimensional crystal, the region of negative effective permeability shrinks and disappears for relatively thick slabs. Our analysis demonstrates that the complex photonic band structure is a valuable tool in the study of three-dimensional metamaterials and their effective-medium description.

DOI: 10.1103/PhysRevB.78.165114 PACS number(s): 42.70.Qs, 42.25.Bs, 73.20.Mf, 78.67.Bf

I. INTRODUCTION

In the last years, the optical properties of metal-dielectric-metal nanosandwiches, i.e., pairs of coaxial metallic nanodisks separated by a cylindrical dielectric spacer, attract considerable attention because they exhibit tunable plasmonic resonances. Studies of multilayered gold-silica nanodisks revealed the existence of strong plasmon resonances that can be tailored by varying the thickness of the dielectric layer.[1] Additionally, it was shown that a pair of gold nanodisks stacked in a sandwichlike configuration, with a dielectric in between, produces large enhancement of the magnetic field when irradiated with a plane optical wave of appropriate frequency, if the distance between the nanodisks is optically small, an effect which can be rationalized in terms of a magnetic-dipole resonance.[2] Moreover, systematic investigations of two-dimensional (2D) arrays of gold-silica-gold nanosandwiches on a dielectric substrate revealed a bimodal resonant response at optical frequencies due to plasmon hybridization. The degree of electromagnetic (EM) coupling in the system can be controlled by varying the aspect ratio of one of the disks in the layered particle.[3,4] Such structures can be synthesized in the laboratory using modern self-assembly and lithographic techniques and provide impressive opportunities for tailoring the light-matter interaction. The particle-plasmon modes of the individual metallic nanodisks of the nanosandwich interact with each other and give rise to a symmetric and an antisymmetric resonant optical mode, by analogy to the formation of bonding and antibonding electron orbitals in diatomic molecules.[5] In this respect, metal-dielectric-metal nanosandwiches constitute a class of photonic metamolecules. In their symmetric optical mode, the electron gas oscillates in phase in the two metallic nanodisks. In the antisymmetric one, these oscillations have opposite phase, leading effectively to an electric current nanoloop that corresponds to a magnetic-type resonance, which is an essential ingredient in the design of negative-index metamaterials at visible and near-infrared frequencies.[6–8]

Metal-dielectric-metal nanosandwiches have been theoretically investigated by means of electrodynamic simulations based on the discrete-dipole-approximation[1] and the finite-difference time-domain[2–4] methods. However, a systematic theoretical study of the optical response of periodic structures of such composite nanoparticles, through full-electrodynamic calculations that take also into account the presence of a supporting substrate, is still missing. In the present paper we employ an extended version of the layer-multiple-scattering method[9–12] to study the optical response of hexagonal arrays of silver-silica-silver nanosandwiches on a quartz substrate. We analyze corresponding extinction spectra and examine the influence of geometrical parameters of the structure, such as lattice constant and size of nanodisks, on the collective plasmonic excitations of the system. We also evaluate the effective electric permittivity and magnetic permeability, and examine their dependence on the above parameters. In addition, we investigate the optical properties of stacks of successive layers of such composite particles that build a fcc crystal and discuss general requirements the complex photonic band structure must fulfill in order for an effective-medium description to be valid.

II. PLASMON HYBRIDIZATION IN A METAL-DIELECTRIC-METAL NANOSANDWICH

The metallic nanodisks, which constitute the building units of a nanosandwich, are characterized by a (relative) magnetic permeability $\mu_s=1$ and a (relative) electric permittivity ϵ_s. We assume, to begin with, that ϵ_s has the simple yet effective Drude form[13]

$$\epsilon_s(\omega) = 1 - \frac{\omega_p^2}{\omega(\omega + i\tau^{-1})}, \tag{1}$$

where ω_p is the bulk plasma frequency and τ is the relaxation time of the conduction-band electrons of the metal, which accounts for dissipative losses. When using the Drude permittivity of Eq. (1), it is convenient to express the frequency in units of ω_p and consider c/ω_p as the length unit, where c is the velocity of light in vacuum. We note that, assuming a

typical value of 10 eV for $\hbar\omega_p$, c/ω_p corresponds to about 20 nm.

A detailed analysis of the particle-plasmon modes of metallic nanodisks has been reported elsewhere.[14] Here, we restrict ourselves to noting that the optical response of such a single nanodisk, in air, is dominated by the fundamental particle-plasmon resonance, which is predominantly of dipole electric type. If the nanodisk is described, for example, by the Drude permittivity given by Eq. (1) without dissipative losses ($\tau^{-1}=0$) and has a radius $S=2.5c/\omega_p$ and a thickness $h=c/\omega_p$, the resonance frequency is at $0.293\omega_p$. For a silver disk of dimensions $S=50$ nm and $h=20$ nm, described by the bulk permittivity of silver measured by Johnson and Christy[15] that includes dissipative losses, the resonance appears at 2.51 eV.

In a metal-dielectric-metal nanosandwich, the interaction between the particle-plasmon modes of the constituent metallic disks results into a symmetric high-frequency hybrid mode (the electric field oscillates in phase in the two metallic nanodisks normal to their axis) and an antisymmetric low-frequency hybrid mode (the electric field oscillates with opposite phase in the two metallic nanodisks normal to their axis). This particle-plasmon hybridization can be analyzed in the light of a simple model of two interacting point dipoles.[2,4,7,8] The electric field at $\mathbf{r}=r\hat{\mathbf{r}}$ from a point dipole $\mathbf{p}$ which oscillates with an angular frequency ω, assuming an $\exp(-i\omega t)$ time dependence, is[16]

$$\mathbf{E}(\mathbf{r})=\left[\left(1-\frac{i\omega r}{c}\right)\frac{3(\hat{\mathbf{r}}\cdot\mathbf{p})\hat{\mathbf{r}}-\mathbf{p}}{r^3}+\frac{\omega^2}{c^2}\frac{\mathbf{p}-(\hat{\mathbf{r}}\cdot\mathbf{p})\hat{\mathbf{r}}}{r}\right]\exp(i\omega r/c). \tag{2}$$

We note that Eq. (2) takes fully into account retardation effects. For a pair of point dipoles, $\mathbf{p}_1$ and $\mathbf{p}_2$, separated by a distance $\mathbf{R}$, in the absence of external field, the field at each dipole is the field due to the other dipole. On the other hand, the induced moment on each dipole is the polarizability, $\alpha(\omega)$, times this field. Therefore, the normal modes of the system for $\mathbf{p}_1\|\mathbf{p}_2$ and $\mathbf{R}\perp\mathbf{p}_{1,2}$ (nanosandwich configuration) are obtained from the linear system of homogeneous equations

$$f(\omega,R)p_1+g(\omega,R)p_2=0$$

$$g(\omega,R)p_1+f(\omega,R)p_2=0, \tag{3}$$

where $f(\omega,R)=(1-i\omega R/c-\omega^2R^2/c^2)\exp(i\omega R/c)$ and $g(\omega,R)=R^3/\alpha(\omega)$. Obviously, Eq. (3) accepts a symmetric ($p_1=p_2$) and an antisymmetric ($p_1=-p_2$) solution, for $f(\omega,R)+g(\omega,R)=0$ and $f(\omega,R)-g(\omega,R)=0$, respectively. These equations ensure the existence of nontrivial solutions of Eq. (3) and their roots in the lower complex-frequency half-plane define the eigenfrequencies of the symmetric and antisymmetric mode, respectively.

The resonant response of the metallic nanodisks is captured in the frequency dependence of the electric polarizability tensor. In the present case, only the transversal (normal to the disk axis) element of this tensor is relevant. Unfortunately, no closed-form solutions exist for the polarizability of the disk. However, it has been shown by means of numerical calculations that the polarizability of a disk is close to that of a spheroid with the same aspect ratio and permittivity,[17] i.e.,

$$\alpha(\omega)=\frac{V}{4\pi}\frac{\epsilon_s(\omega)-1}{1+L[\epsilon_s(\omega)-1]}, \tag{4}$$

where V is the volume of the particle and $0<L<1$ is the depolarization factor ($L=1/3$ for a sphere). We assume, for simplicity, that $\epsilon_s(\omega)$ has the simple Drude form of Eq. (1) and choose for the damping factor the typical value $\tau^{-1}=0.1\omega_p$ to account for absorptive and radiative losses.[18] Considering nanodisks of thickness c/ω_p and radius $2.5c/\omega_p$, a depolarization factor of $L=0.085\,85$ was assumed in order to match the calculated eigenfrequency $\sqrt{L}\omega_p=0.293\omega_p$ of the lowest particle-plasmon mode which is relevant here. The variation in the complex eigenfrequencies of the coupled dipoles versus their separation, obtained through Eq. (3), is depicted in Fig. 1. It can be seen that hybridization leads to a low-frequency antisymmetric and a high-frequency symmetric mode. The corresponding eigenfrequencies at relatively large dipole-dipole separations are close to that of the isolated nanodisk, while level repulsion becomes more prominent as the two dipoles approach each other and, consequently, hybridization increases.

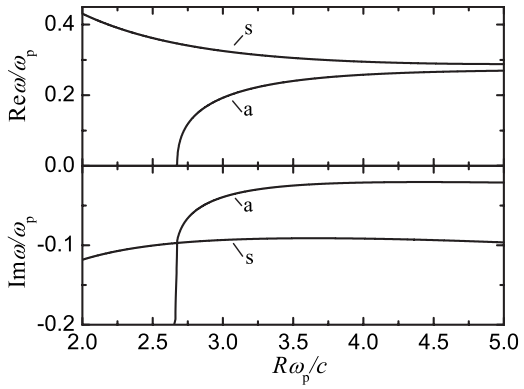

FIG. 1. Plasmon hybridization in a metal-dielectric-metal nanosandwich: variation in the complex eigenfrequencies of the symmetric (s) and antisymmetric (a) modes in a simple model of coupled dipoles as a function of their separation. The permittivity of the metal is given by Eq. (1), with $\tau^{-1}=0.1\omega_p$

III. PLANAR STRUCTURES OF METAL-DIELECTRIC-METAL NANOSANDWICHES

We now apply the extended layer-multiple-scattering method to study the plasmonic excitations of hexagonal arrays of silver-silica-silver nanosandwiches on a quartz substrate ($\epsilon_{\text{quartz}}=2.13$, $\mu_{\text{quartz}}=1$). A periodic array of nanosandwiches is built of three consecutive layers of appropriate nanodisks, through the proper combination of the transmission and reflection matrices of the component layers.[9–12] For the permittivity of silver we interpolate to the bulk values measured by Johnson and Christy[15] while for silica we assume a permittivity of 2.13. In order to ensure adequate convergence in our calculations, we truncate the spherical-wave expansions at $\ell_{\max}=15$ and take into account

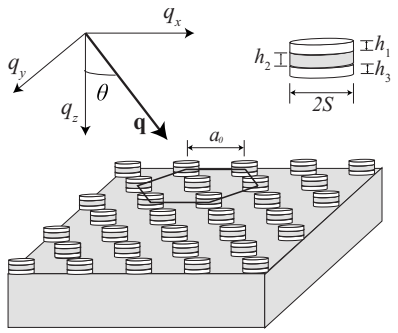

FIG. 2. Schematic view of a hexagonal array of silver-silica-silver nanosandwiches on a quartz substrate.

151 reciprocal-lattice vectors in the relevant plane-wave expansions, while the scattering T matrix of the single nanodisk is calculated with $\ell_{\text{cut}}=20$ and a Gaussian quadrature integration formula with 6000 points.[12] We consider nanosandwiches of radius $S=50$ nm and typical thickness $h_1=20$ nm silver, $h_2=40$ nm silica and $h_3=20$ nm silver, arranged on a hexagonal lattice with lattice constant $a_0=250$ nm (see Fig. 2). Such large interparticle separations essentially correspond to isolated particles as we discuss below.

In order to study the hybridization between the particle-plasmon modes of the two metallic nanodisks of the nanosandwich, we keep their thickness fixed ($h_1=h_3=20$ nm) and vary the thickness h_2 of the dielectric spacer. Corresponding extinction spectra (extinction=negative logarithm of the transmittance) at normal incidence are depicted in the upper panel of Fig. 3. For very thin dielectric spacers, the extinction spectrum tends to a single-peak structure, which is essentially the particle-plasmon resonance in the corresponding array of homogeneous silver disks 40 nm thick. On the other hand, when the separation between silver disks in the nanosandwich is larger (typically >10 nm), the spectra exhibit two distinct peaks. With increasing thickness of the dielectric spacer, the high-frequency peak shifts to the

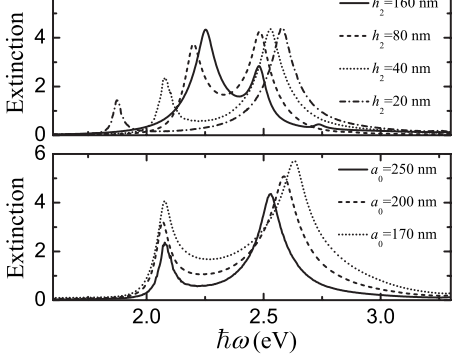

FIG. 3. Extinction at normal incidence of hexagonal arrays of silver-silica-silver nanosandwiches with radius $S=50$ nm and thickness of the silver disks $h_1=h_3=20$ nm, on a quartz substrate. Upper panel: lattice constant $a_0=250$ nm. The different spectra correspond to silica spacer thicknesses $h_2=160$, 80, 40, and 20 nm. Lower panel: silica spacer thickness $h_2=40$ nm. The different spectra correspond to lattice constants $a_0=250$, 200, and 170 nm.

red while the low-frequency peak shifts to the blue and gradually becomes more pronounced. Interestingly, when the separation between silver disks is small (<10 nm) the low-frequency peak is not observed. Our results are in good agreement with existing experimental data on isolated gold-silica-gold nanosandwiches[1,3] and can be explained as follows. The double-peak structure in the calculated extinction spectra results from the excitation of the composite plasmon modes of the individual nanosandwiches, weakly interacting between them. It is worth noting that the shift of the antisymmetric mode is larger than that of the symmetric mode, in agreement with the results of the model calculations shown in Fig. 1. Moreover, as can be seen in Fig. 1, while the imaginary part of the eigenfrequency of the symmetric mode remains practically constant, the eigenfrequency of the antisymmetric mode moves rapidly away from the real axis in the lower complex-frequency half-plane, thus implying a drastic reduction in the lifetime of this mode as the distance between the dipoles decreases, which is in line with the suppression of the corresponding peak in the extinction spectra shown in the upper panel of Fig. 3. The interaction between nanosandwiches increases as we reduce the lattice constant and is manifested as a small shift of the resonance peaks and more pronounced extinction, as can be seen in the lower panel of Fig. 3.

In the case of the planar structures under consideration, using the point-dipole model of Sec. II, the evaluation of the local field at a given dipole $\mathbf{p}_0$ involves an infinite sum over all other dipoles $\mathbf{p}_n$ at sites $\mathbf{R}_n \neq \mathbf{0}$. Because of the periodicity of the structure, the component of the wave vector parallel to the plane of nanosandwiches, reduced within the surface Brillouin zone of the given 2D lattice, $\mathbf{k}_\parallel$, is an invariant. Taking advantage of Bloch theorem $\mathbf{p}_n=\mathbf{p}_0 \exp(i\mathbf{k}_\parallel \cdot \mathbf{R}_n)$ and assuming that the resonant response of the individual nanosandwiches can be described through an electric or magnetic polarizability function, we obtain a secular equation which gives the (complex) eigenfrequencies of the system for a given value of $\mathbf{k}_\parallel$.[19,20] In general, we obtain two relatively narrow bands of resonant modes, $\omega(\mathbf{k}_\parallel)$, about the eigenfrequencies of the antisymmetric and symmetric modes, respectively, of the single nanosandwich. The modes corresponding to $\mathbf{k}_\parallel=\mathbf{0}$ are those which are excited at normal incidence. Reducing the lattice constant of the structure, the increased coupling strength leads to a larger band width[13] and thus to a corresponding shift of $\omega(\mathbf{0})$, which explains the shift of the resonance peaks in the lower panel of Fig. 3. It is worth noting that, though the near-field interactions play the dominant role in the nearest-neighbor coupling at short lattice constants, far-field interactions, also with more distant neighbors, are important.[21]

We now want to describe the array of nanodisks under consideration by an equivalent homogeneous slab, of thickness D, effective permittivity ϵ_{eff} and effective permeability μ_{eff}. For this purpose, we invert the standard Fresnel equations which give the transmission and reflection coefficients, t and r, respectively, of a homogeneous slab described by a refractive index n_2 and an impedance z_2, placed between two semi-infinite homogeneous media with n_1, z_1 and n_3, z_3.[22,23] Obviously, this procedure takes also into account the presence of the substrate. At normal incidence, the impedance

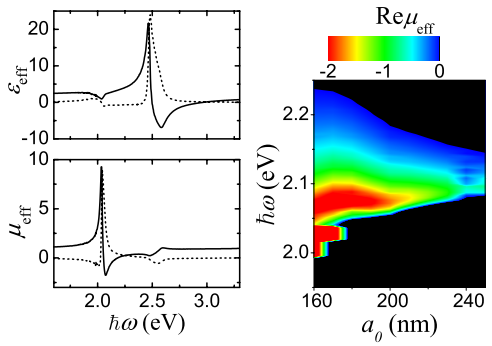

FIG. 4. (Color online) Left-hand panel: real (solid lines) and imaginary (dashed lines) part of the effective permittivity, ϵ_{eff}, and permeability, μ_{eff}, of a hexagonal array, with lattice constant $a_0=200$ nm, of silver-silica-silver nanosandwiches, with $S=50$ nm, $h_1=h_3=20$ nm, and $h_2=40$ nm, on a quartz substrate. Right-hand panel: a map of the negative effective permeability of different hexagonal arrays of the nanoparticles described above.

and the refractive index of the slab can be retrieved through

$$z_2 = \pm \frac{\sqrt{(r-1)^2 - t^2} z_1 z_3}{\sqrt{(r+1)^2 z_3^2 - t^2 z_1^2}} \tag{5}$$

and

$$\tan(\beta/2) = \pm i \sqrt{\frac{(r-1+t)[z_3(r+1)-tz_1]}{(r-1-t)[z_3(r+1)+tz_1]}}, \tag{6}$$

respectively, where $\beta=(\omega/c)n_2D$. The sign in Eq. (5) is unambiguously determined by the condition Re $z_2>0$, required for a passive medium. Moreover, to ensure an exponential decay of an outgoing wave, the imaginary part of β has to be always positive, which fixes the sign in Eq. (6). The effective permittivity and permeability of the slab are given by $\epsilon_{\text{eff}}=n_2/z_2$ and $\mu_{\text{eff}}=n_2z_2$.

As an application, we consider a hexagonal array, with lattice constant $a_0=200$ nm, of silver-silica-silver nanosandwiches, with $h_1=h_3=20$ nm, $h_2=40$ nm, and $S=50$ nm, on a quartz substrate. It is reasonable to take the effective thickness of the homogeneous slab equal to the total thickness of the nanosandwich, $D=80$ nm, though other choices for D (>80 nm) do not alter much our results. The effective parameters ϵ_{eff} and μ_{eff} retrieved by the method described above are shown in the left-hand panel of Fig. 4. One observes a resonance in the permeability in the frequency region of the antisymmetric mode and a similar resonance in the permittivity in the frequency region of the symmetric mode. Interestingly, the resonance in the permittivity is accompanied by a small resonance structure in the permeability, and vice versa, which indicates that these resonances are not of solely electric or magnetic type. We obtain a negative effective permeability as large as -1.77 in the frequency region between 2.05 and 2.18 eV, and a negative effective permittivity in the frequency region between 2.50 and 2.97 eV. However, these negative values are accompanied by relatively high losses, with the imaginary part of the refractive index being as high as 2.5. The corresponding transmission spectrum is characterized by two local minima, as low as 4% and 0.5%, near the resonance frequencies of the antisymmetric and symmetric modes about 2.1 and 2.7 eV, respectively. Enhanced absorption, of the order of 40% and 16%, respectively, is obtained about the two resonance frequencies, as expected for plasmonic resonances in metallodielectric structures.

The right-hand panel of Fig. 4 displays the real part of the effective magnetic permeability, Re μ_{eff}, versus the lattice constant of hexagonal arrays of the nanosandwiches described above, in the frequency region where Re $\mu_{\text{eff}}<0$. As we have already discussed in relation to Fig. 3, as we reduce the lattice constant, the interaction between nanosandwiches is stronger, resulting to more pronounced resonance structures in the extinction spectrum and more negative Re μ_{eff} within a broader frequency region.

IV. THREE-DIMENSIONAL CRYSTALS OF METAL-DIELECTRIC-METAL NANOSANDWICHES

Let us consider the general case of a photonic crystal made of scatterers which exhibit localized resonances, of electric or magnetic type, in a homogeneous host medium. We view the crystal as an infinite succession of consecutive layers, separated by a distance d, parallel to a given crystallographic plane which is taken to be the xy plane. We neglect dissipative losses in the constituent materials in order to ensure an unambiguous interpretation of the corresponding frequency band structure. In such a photonic crystal, the resonant modes of the individual scatterers interact weakly between them and form narrow bands of collective modes, which hybridize with the extended band that would be in a homogeneous effective medium in the absence of resonant modes. As a result, a frequency gap opens up about the crossing point of these bands and is referred to as hybridization gap by analogy to the $s-d$ hybridization gap in the electron band structure of transition metals.[13] In the gap region there are no propagating modes of the EM field and the real-frequency dispersion lines continue analytically in the complex k_z plane.[24] In principle, there is an infinite number of such complex bands but, over a gap region, it is the complex band of the appropriate symmetry with the smallest in magnitude imaginary part of k_z which determines the attenuation of EM waves through a finite slab of the crystal, along the given direction. Obviously, in the example shown in the upper panel of Fig. 5, the relevant complex band near the top of the gap, at the Brillouin-zone center, has Re $k_z=0$ and that near the bottom of the gap, at the Brillouin-zone edge, has Re $k_z=\pi/d$. It is interesting to examine whether such a complex band diagram of a photonic crystal can be associated to a homogeneous effective medium, at wavelengths long enough compared to the size of the particles and the lattice spacing. The presence of collective electric or magnetic resonances in the crystal implies a resonant behavior of the effective permittivity, ϵ_{eff}, or permeability, μ_{eff}, functions, respectively,[25–29] as shown in the lower panel of Fig. 5. Since there are no dissipative losses, the resonant response function (either ϵ_{eff} or μ_{eff}) is real and exhibits an asymptotic variation taking negative values within a frequency interval next to the asymptote. In this region, assuming that the other

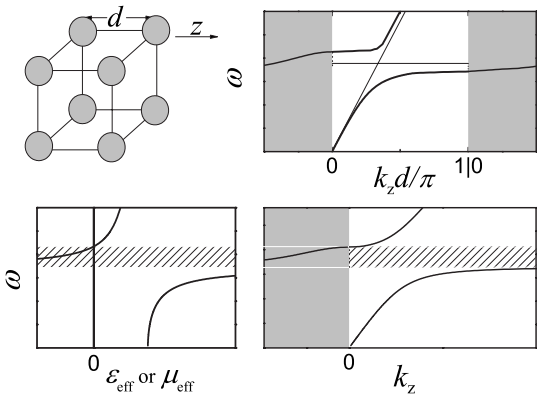

FIG. 5. Upper panel: a photonic crystal of resonant units (left) and a typical schematic example of its complex band structure along a given (z) direction (right). In the gap region, Re k_z is shown by dotted lines and Im k_z is plotted in the gray-shaded areas. The thin lines show the extended and resonance bands, in the absence of hybridization between them. Lower panel: the corresponding effective-medium resonant permittivity or permeability (left) and complex band structure (right). The hatched region marks the frequency gap.

(nonresonant) response function is real and positive, there can be no propagating modes of the EM field. We have there a frequency gap, over which $k=(\epsilon_{\rm eff}\mu_{\rm eff})^{1/2}\omega/c$ is purely imaginary (Re $k=0$). We note in passing that, if both $\epsilon_{\rm eff}$ and $\mu_{\rm eff}$ are negative over a given frequency region, k becomes real and we have a negative-index behavior. On the other hand, if absorption is taken into account, k takes complex values. A clear picture can be obtained if dissipative losses are neglected. Recalling the corresponding band structure of the actual photonic crystal, we see that the dominant evanescent modes near the top of the gap correspond, indeed, to Re $k_z=0$. Consequently, the form of the associated Bloch envelope wave functions ($\exp[-\text{Im}\, k_z nd]$) is compatible with that of the evanescent modes supported in the effective medium, in the frequency region of negative $\epsilon_{\rm eff}\mu_{\rm eff}$. On the contrary, near the bottom of the gap, the dominant evanescent modes, resulting from destructive wave interference through multiple scattering in the periodic array of scatterers, correspond to Re $k_z\neq 0$, and such waves cannot be formed in the effective medium. It becomes clear from the above that a necessary condition for the definition of a negative-permittivity or negative-permeability nondissipative 3D metamaterial is the existence of a gap region where the proper real-frequency line with the smallest $|\text{Im}\, k_z|$ has Re $k_z=0$. This conclusion is in agreement with recent studies which show that the validity of the effective-medium description of photonic crystals is restricted by the accuracy of the single-mode approximation.[30,31]

We now consider a fcc crystal, built as a sequence of (111) planes of nanosandwiches consisting of two metallic nanodisks, of radius $S=2.5c/\omega_p$ and thickness $h_1=h_3=c/\omega_p$, separated by a silica spacer of thickness $h_2=2c/\omega_p$. The crystal has a lattice constant $a=\sqrt{2}a_0=10\sqrt{2}c/\omega_p$ and the distance between successive (111) planes is $d=a\sqrt{3}/3$. We assume that the permittivity of the metallic disks is described by Eq. (1), and we deliberately disregard absorption ($\tau^{-1}=0$) in order to be able to calculate the frequency band structure in an unambiguous manner. The left-hand panel of Fig. 6 shows the corresponding photonic band structure along the [111] direction. At low frequencies we obtain a doubly degenerate linear dispersion curve, as expected for propagation in a homogeneous medium characterized by a frequency-independent effective refractive index. At higher frequencies the band structure is dominated by flat, almost dispersionless bands, which originate from the antisymmetric and symmetric plasmon modes of the nanosandwiches, about $0.24\omega_p$ and $0.35\omega_p$, respectively. These resonance bands hybridize with the extended band that would be in the effective medium to produce the doubly degenerate bands in the photonic crystal shown in the left-hand panel of Fig. 6. The doubly degenerate bands couple with an EM wave incident normally on a (111) slab of this crystal, leading to measurable transmittance, as shown in the right-hand panel of Fig. 6.

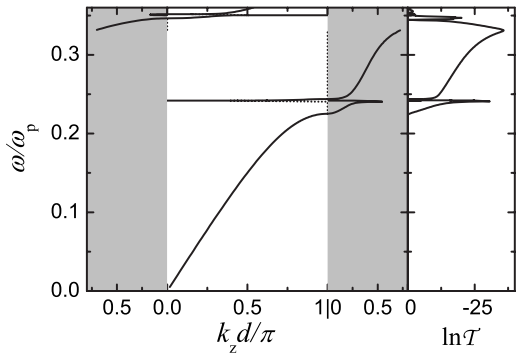

FIG. 6. Left-hand panel: the photonic band structure of a fcc crystal, with lattice constant $a=10\sqrt{2}c/\omega_p$, of nanosandwiches consisting of two metallic disks of radius $S=2.5c/\omega_p$ and thickness $h_1=h_3=c/\omega_p$, separated by a silica spacer of thickness $h_2=2c/\omega_p$, in air, along the [111] direction. The permittivity of the metallic disks is described be Eq. (1), with $\tau^{-1}=0$. Apart from the ordinary frequency bands (k_z is real), we also show, over the gap regions, the doubly degenerate real-frequency lines for the complex eigenvalues k_z with the smallest in magnitude imaginary part (Re k_z is shown by dotted lines and Im k_z is plotted in the gray-shaded areas). Right-hand panel: transmittance at normal incidence of a slab of $N_L=8$ (111) planes of the above crystal, in logarithmic scale.

As can be seen in the left-hand panel of Fig. 6, sizeable gaps open up in the frequency band structure of the photonic crystal under consideration. Over the gap regions we show the real-frequency lines for complex eigenvalues k_z that correspond to the doubly degenerate bands with the smallest in magnitude imaginary part (plotted in the grey-shaded areas). These lines are the analytic continuations in the complex k_z plane of the bands below and above the gaps and determine the attenuation of the wave field over these regions; $\ln\mathcal{T}(\omega)=-2dN_L\,\text{Im}\,k_z(\omega)+\text{const}$, for a given value of $\mathbf{k}_\parallel$.[32] This is indeed observed in the right-hand panel of Fig. 6, where we show the logarithm of the transmittance for a wave incident normally on a slab of the given crystal consisting of $N_L=8$ (111) planes. Interestingly, in the frequency region of the antisymmetric plasmon modes of the nanosandwiches, there is no gap region where the relevant complex band has Re $k_z=0$. This implies that the given 3D crystal does not exhibit a negative effective permeability. It is worth noting

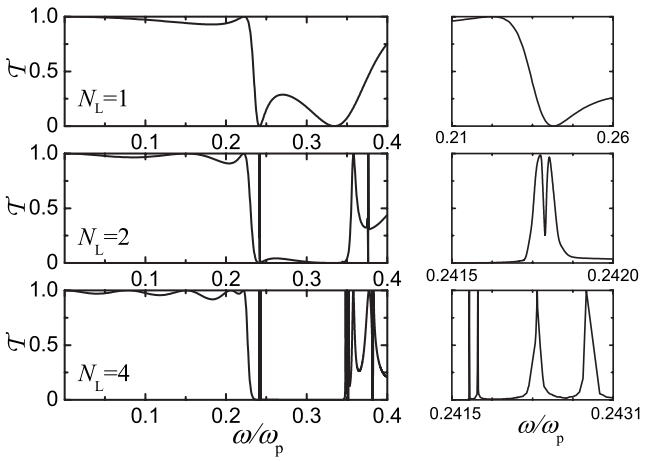

FIG. 7. Transmittance at normal incidence of finite slabs consisting of $N_L=1$, 2, and 4 (111) planes of the photonic crystal of Fig. 6. Resonance structures originating from the antisymmetric plasmonic modes of the nanosandwiches are shown with a higher resolution in the right-hand panel.

that, for a single (111) plane of this crystal, we retrieve a negative effective permeability, as large as −0.18, between $0.240\omega_p$ and $0.254\omega_p$. However, as we add successive layers in order to build the fcc crystal under consideration, this region shrinks and finally disappears for relatively thick slabs, due to multiple scattering between the layers. This finding also holds for a quite wide range of lattice constants, as we verified by systematic numerical calculations. On the other hand, the existence of a gap region, just below the flat band of symmetric modes, where the doubly degenerate complex band with the smallest $|\mathrm{Im}\ k_z|$ has $\mathrm{Re}\ k_z=0$ is consistent with a negative-permittivity effective-medium behavior in this frequency region, which subsists as we grow the photonic crystal layer by layer.

The evolution of the frequency band structure of the photonic crystal under consideration by increasing the number of layers, N_L, is depicted in Fig. 7. The transmittance over the region of the extended band in the left-hand panel of Fig. 6 exhibits the well-known Fabry-Pérot oscillations due to multiple scattering between the surfaces of the slab. The maxima of these oscillations appear at frequencies ω_n, which correspond exactly to discrete values of the wave number $k_z=n\pi/dN_L$, deduced from the associated dispersion line in the left-hand panel of Fig. 6, i.e., when the slab thickness equals an integral multiple of a half Bloch wavelength. The gap regions can be identified as the frequency intervals of practically vanishing transmittance, already in very thin slabs ($N_L>2$). Finally, the Fano resonance structures in the transmittance of the slabs[32] are clearly due to the appropriate collective antisymmetric and symmetric plasmonic modes of the nanosandwiches of the individual layers interacting very weakly between them. It is worth noting the fact that these resonances appear at frequencies along the associated real-frequency line corresponding to $\mathrm{Re}\ k_z=n\pi/d(N_L+1)$, $n=1,2,\ldots,N_L$ in the left-hand panel of Fig. 6, which implies that the number of transmission resonances increases with the thickness of the slab,[33] as shown in the right-hand panel of Fig. 7.

V. CONCLUSIONS

In summary, we reported on the optical response of 2D and 3D ordered arrays of metal-dielectric-metal nanosandwiches, by means of full electrodynamic calculations using the extended layer-multiple-scattering method. In addition, we presented a simple coupled-dipole model that explains plasmon hybridization in a single nanosandwich, enabling physical insight into the formation of a symmetric and an antisymmetric resonance recently reported in the experiment. We showed that the extinction spectrum of planar periodic nanosandwich assemblies on a dielectric substrate is characterized by a double-peak structure, which can be tuned by a proper choice of the geometrical parameters involved. Our results corroborate that such systems, with a tailored optical response, can be useful for practical applications, e.g., as chemical and biological sensors, while the presence of an antisymmetric resonance induces a negative effective permeability, which makes metallodielectric nanosandwiches potential candidates as building units in the design of negative-index metamaterials. However, as successive layers are stacked together to build a fcc crystal, the region of negative effective permeability shrinks and disappears for relatively thick slabs. This leads to the conclusion that one cannot always infer an effective-medium description and deduce the relevant parameters of 3D metamaterials from the response of single layers or even very thin slabs, which agrees with the results of Rockstuhl *et al.*[30] We introduced the complex photonic band structure as a tool in the study of 3D metamaterials and established additional criteria for the validity of their effective-medium description. The present work demonstrates the efficiency and accuracy of our recently developed extended layer-multiple-scattering method in the study of complex 2D and 3D structures of composite metallodielectric nanoparticles of arbitrary shape.

ACKNOWLEDGMENTS

This work was supported by the research program "Kapodistrias" of the University of Athens and by NCSR "Demokritos" under "Demoerevna" Grant No. E-1437.

[1] K. H. Su, Q. H. Wei, and X. Zhang, Appl. Phys. Lett. **88**, 063118 (2006).

[2] T. Pakizeh, M. S. Abrishamian, N. Granpayeh, A. Dmitriev, and M. Käll, Opt. Express **14**, 8240 (2006).

[3] A. Dmitriev, T. Pakizeh, M. Käll, and D. S. Sutherland, Small **3**, 294 (2007).

[4] T. Pakizeh, A. Dmitriev, M. S. Abrishamian, N. Granpayeh, and M. Käll, J. Opt. Soc. Am. B **25**, 659 (2008).

[5] E. Prodan, C. Radloff, N. J. Halas, and P. Nordlander, Science **302**, 419 (2003).
[6] A. N. Grigorenko, A. K. Geim, H. F. Gleeson, Y. Zhang, A. A. Firsov, I. Y. Khrushchev, and J. Petrovic, Nature (London) **438**, 335 (2005).
[7] A. K. Sarychev, G. Shvets, and V. M. Shalaev, Phys. Rev. E **73**, 036609 (2006).
[8] W. Cai, U. K. Chettiar, H. K. Yuan, V. C. de Silva, A. V. Kildishev, V. P. Drachev, and V. M. Shalaev, Opt. Express **15**, 3333 (2007).
[9] N. Stefanou, V. Yannopapas, and A. Modinos, Comput. Phys. Commun. **113**, 49 (1998).
[10] N. Stefanou, V. Yannopapas, and A. Modinos, Comput. Phys. Commun. **132**, 189 (2000).
[11] A. Modinos, N. Stefanou, and V. Yannopapas, Opt. Express **8**, 197 (2001).
[12] G. Gantzounis and N. Stefanou, Phys. Rev. B **73**, 035115 (2006).
[13] W. A. Harrison, *Solid State Theory* (Dover, New York, 1980).
[14] G. Gantzounis, N. Stefanou, and N. Papanikolaou, Phys. Rev. B **77**, 035101 (2008).
[15] P. B. Johnson and R. W. Christy, Phys. Rev. B **6**, 4370 (1972).
[16] J. D. Jackson, *Classical Electrodynamics* (Wiley, New York, 1999).
[17] J. Venermo and A. Sihvola, J. Electrost. **63**, 101 (2005).
[18] K. H. Fung and C. T. Chan, Opt. Commun. **281**, 855 (2008).
[19] F. J. García de Abajo, Rev. Mod. Phys. **79**, 1267 (2007).
[20] M. Englund and A. Viitanen, Microwave Opt. Technol. Lett. **49**, 2419 (2007).
[21] A. F. Koenderink and A. Polman, Phys. Rev. B **74**, 033402 (2006).
[22] D. R. Smith, S. Schultz, P. Markos, and C. M. Soukoulis, Phys. Rev. B **65**, 195104 (2002).
[23] C. Menzel, C. Rockstuhl, T. Paul, F. Lederer, and T. Pertsch, Phys. Rev. B **77**, 195328 (2008).
[24] V. Heine, Proc. Phys. Soc. London **81**, 300 (1963).
[25] R. Ruppin, Opt. Commun. **182**, 273 (2000).
[26] M. S. Wheeler, J. S. Aitchison, and M. Mojahedi, Phys. Rev. B **72**, 193103 (2005).
[27] M. S. Wheeler, J. S. Aitchison, and M. Mojahedi, Phys. Rev. B **73**, 045105 (2006).
[28] V. Yannopapas and A. Moroz, J. Phys.: Condens. Matter **17**, 3717 (2005).
[29] V. Yannopapas and N. V. Vitanov, Phys. Rev. B **74**, 193304 (2006).
[30] C. Rockstuhl, T. Paul, F. Lederer, T. Pertsch, T. Zentgraf, T. P. Meyrath, and H. Giessen, Phys. Rev. B **77**, 035126 (2008).
[31] W. Śmigaj and B. Gralak, Phys. Rev. B **77**, 235445 (2008).
[32] G. Gantzounis and N. Stefanou, Phys. Rev. B **72**, 075107 (2005).
[33] N. Liu, H. Guo, L. Fu, S. Kaiser, H. Schweizer, and H. Giessen, Adv. Mater. (Weinheim, Ger.) **19**, 3628 (2007).